Measurement of the free neutron lifetime in a magneto-gravitational trap with *in situ* detection

R. Musedinovic,[1] L. S. Blokland,[2] C. B. Cude-Woods,[3] M. Singh,[3] M. A. Blatnik,[3,4] N. Callahan,[5] J. H. Choi,[1] S. M. Clayton,[3,*] B. W. Filippone,[4] W. R. Fox,[2] E. Fries,[4] P. Geltenbort,[6] F. M. Gonzalez,[7] L. Hayen,[1] K. P. Hickerson,[4] A. T. Holley,[8] T. M. Ito,[3] A. Komives,[9] S. Lin,[3] Chen-Yu Liu,[10] M. F. Makela,[3] C. M. O'Shaughnessy,[3] R. W. Pattie, Jr.,[11] J. C. Ramsey,[7] D. J. Salvat,[2] A. Saunders,[7] S. J. Seestrom,[3] E. I. Sharapov,[12] Z. Tang,[3] F. W. Uhrich,[3] J. Vanderwerp,[2] P. Walstrom,[3] Z. Wang,[3] A. R. Young,[1,13] and C. L. Morris[3]

[1]*Department of Physics, North Carolina State University, Raleigh, North Carolina 27695, USA*
[2]*Department of Physics, Indiana University, Bloomington, Indiana 47405, USA*
[3]*Los Alamos National Laboratory, Los Alamos, New Mexico 87545, USA*
[4]*Kellogg Radiation Laboratory, California Institute of Technology, Pasadena, California 91125, USA*
[5]*Argonne National Laboratory, Lemont, Illinois 60439, USA*
[6]*Institut Laue-Langevin, CS 20156, 38042 Grenoble Cedex 9, France*
[7]*Oak Ridge National Laboratory, Oak Ridge, Tennessee 37831, USA*
[8]*Tennessee Technological University, Cookeville, Tennessee 38505, USA*
[9]*DePauw University, Greencastle, Indiana 46135, USA*
[10]*University of Illinois, Urbana, Illinois 61801, USA*
[11]*East Tennessee State University, Johnson City, Tennessee 37614, USA*
[12]*Joint Institute for Nuclear Research, 141980 Dubna, Russia*
[13]*Triangle Universities Nuclear Laboratory, Durham, North Carolina 27708, USA*

(Received 6 September 2024; revised 25 November 2024; accepted 18 February 2025; published 7 April 2025)

Here we publish three years of data from the UCNτ experiment performed at the Los Alamos Ultracold Neutron Facility at the Los Alamos Neutron Science Center. These data are in addition to our previously published data. Our goals in this paper are to better understand and quantify systematic uncertainties and to improve the lifetime statistical precision. We previously reported a value from our 2017–2018 data for the neutron lifetime of 877.75 ± 0.28 (statistical) +0.22–0.16 (systematic) s. We have collected an additional three years of data reported here for the first time. When all the data from UCNτ are averaged for 2017, 2018, 2020, 2021, and 2022, we report an updated value for the lifetime of 877.83 ± 0.22 (statistical)+0.20–0.17 (systematic) s. We utilized improved monitor detectors, reduced our correction due to UCN upscattering on residual gas, and employed four different UCN detector geometries both to reduce the correction required for rate dependence and to explore potential contributions due to phase space evolution.

DOI: 10.1103/PhysRevC.111.045501

I. INTRODUCTION

The decay of the free neutron $n \to p + e^- + \bar{\nu}_e$ is one of the simplest examples of nuclear β-decay, and measurements of decay observables have implications for the standard model of particle physics and cosmology. The mean neutron lifetime, τ_n, is needed as an input to predict primordial light element abundances [1]. The combination of the lifetime and neutron decay correlation parameters tests the *V-A* structure of the weak interaction without complications from nuclear structure corrections [2]. Recent and forthcoming neutron β-decay experiments can be used to extract the magnitude of the Cabibbo-Kobayashi-Maskawa (CKM) matrix element $V_{\rm ud}$ with a precision approaching that from studies of super-allowed $0^+ \to 0^+$ nuclear β-decays. Further, these tests can probe for the existence of beyond-standard-model interactions that could evade detection in high-energy collider experiments [3,4].

The history of τ_n measurements, as well as the evaluations by the Particle Data Group (PDG) [5], are plotted in Fig. 1. The present work reports additional results of an experiment [6] to measure τ_n with smaller systematic corrections than previous efforts and using a blinded analysis to avoid confirmation bias. The new data reported here were acquired in 2020, 2021, and 2022 at the Los Alamos Ultracold Neutron Facility [7,8] at the Los Alamos Neutron Science Center (LANSCE).

In the standard model, the following relationship holds [13]:

$$\tau_n^{-1} = \frac{m_e^5}{2\pi^3} G_F^2 |V_{\rm ud}|^2 \left(1 + 3g_A^2\right)(1 + {\rm RC}) f, \qquad (1)$$

where G_F is the Fermi coupling constant, g_A is the neutron weak axial-current coupling, f is a decay phase-space factor, and RC represents the electroweak radiative corrections.

*Contact author: sclayton@lanl.gov

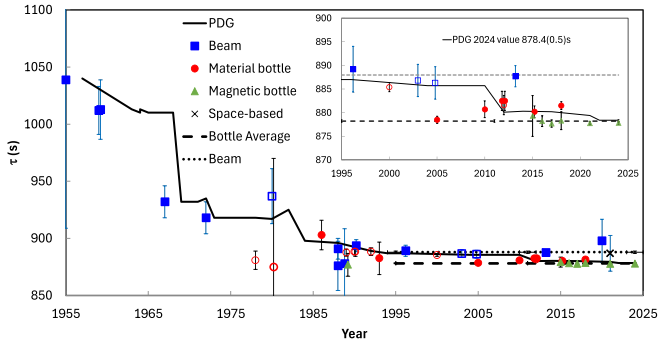

FIG. 1. The history of neutron lifetime measurements and the evaluated neutron lifetime [5,9–12]. The open points have been withdrawn or superseded. The x symbol is from a space-based measurement [12]. The inset shows the most recent results on an expanded scale. Recent measurements using new techniques have large uncertainties and are not included in the inset.

The "inner" radiative correction contains model-dependent hadronic structure and short-distance QCD physics and is the dominant source of theoretical uncertainty in Eq. (1) [13,14].

Steady refinement of the theoretical analysis of the standard model expectations [14–20] for charged current decays of kaons, neutrons, and nuclei has produced strong evidence for discrepancies between the decay observables and standard model expectations collectively referred to as the Cabibbo angle anomaly (CAA) [21,22]. Violation of the expected unitarity of the top row of the CKM matrix appear at roughly the 3σ level or more in these data. Analysis of the CAA in a model-independent framework using effective field theory [23] now incorporates low energy observables such as the neutron lifetime, electroweak precision observables from the Large Electron-Positron collider (LEP), and the recent measurement of the W mass [24], in addition to constraints from the Large Hadron Collider. With this approach, Ref. [23] identifies potential new physics originating from right-handed currents [23] or vector-like quarks [25]. Several other scenarios have been studied. Ref. [26], for example, presents analysis of the CAA incorporating data from the decay of bottom-quarks and the muon anomalous magnetic moment that points to new physics from leptoquarks [27].

Discriminating between these model scenarios requires significant improvement in the current experimental observables. Neutron β-decay data can play a crucial role in these analyses by reducing uncertainties in the input value for the V_{ud} parameter due to nuclear structure uncertainties associated with superallowed nuclear beta decays [18,20,28,29]. This theoretical work increases the motivation for improving the accuracy in both neutron lifetime and beta decay correlations.

Measurements of τ_n are generally performed using either the so-called "beam" or "bottle" technique. The beam technique consists of passing a slow neutron beam through a decay volume of known length and cross-sectional area, and counting neutron decay products (e^-, p, or both) within that volume. With an absolute measurement of the neutron flux and absolute determination of the detector efficiencies, the partial neutron decay rate for neutrons that produce the detected decay product in the final state can be determined. By far the most precise of these beam experiments uses a quasi-Penning trap and silicon surface-barrier detector to count protons from a cold neutron beam at the National Institute of Standards and Technology, NIST [30]. The most recent evaluation gives $\tau_n = 887.7 \pm 1.2[\text{stat}] \pm 1.9[\text{syst}]$ s [10].

The "bottle" technique consists of introducing ultracold neutrons (UCN) with kinetic energy $E \leqslant 100$ neV into a material or magnetic bottle, storing the UCN for varying times, and counting the surviving neutrons to determine the storage lifetime. The most precise measurements using material bottles differ from the NIST experiment by as much as 4.4σ [31–35]. A measurement using a cylindrical magnetic bottle at the Institut Laue-Langevin (ILL) [36] and measurements with the UCNτ apparatus, an asymmetric bowl-shaped magnetic trap at Los Alamos National Laboratory (LANL), give consistent results that also disagree with the NIST experiment by more than 4σ.

This "neutron lifetime puzzle" [37] indicates either the existence of new physics leading to a decay channel without protons in the final state, or the presence of inadequately assessed or unidentified systematic effects in at least one of the experimental techniques. The former could be induced by the decay of neutrons to dark-matter particles [38], but such decay channels are constrained by the properties of neutron stars [39–41] and by direct searches looking for specific decay signatures [42–44]. The latter indicates a need for new or improved experimental techniques to complement existing approaches and mitigate potential systematic effects.

In the present work, we provide new data of the measurements of τ_n first reported in Ref. [45] using the UCNτ apparatus. The apparatus eliminates losses associated with material UCN bottles and utilizes novel detector technology to develop data-driven assessments of potential systematic effects [46,47]. The analysis reported here is aimed at developing new methods to characterize and reduce systematic effects well below 0.2 s, needed for the upcoming experiment, UCNτ+, that will use a new elevator loading technique to increase the number of loaded UCN by a factor of 5–10.

II. EXPERIMENTAL CONFIGURATIONS

The configuration used for this experiment, shown in Fig. 2, was similar to that in Ref. [6]. We used several monitors to measure and study the UCN fluence; all of the monitor detectors were ^{10}B-coated ZnS:Ag UCN detectors [48]. As in previous years, a UCN conditioning volume (round house or RH) was used to minimize the impact of fast variations in UCN production on UCN loading, especially near the end of the loading period. A significant improvement in normalization was achieved by emptying and counting the UCN remaining in that volume at the end of the fill using the RH dump detector. Our previous work used a detector mounted on a vertical standpipe off a 90° "tee" in the horizontal UCN guide that allowed the detector to be mounted above the top of the trap, thereby sampling the relatively abundant UCN above the 45 neV trap depth but requiring a correction for fill-to-fill variations in the UCN energy spectrum based on other detectors at different elevations. The RH dump detector counts the spectrum in a less biased way: a horizontal absorber ("active cleaner") in the RH above the height of the top of

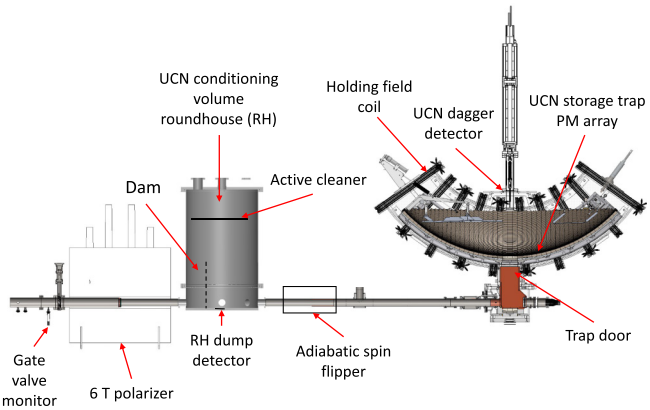

FIG. 2. Experimental layout showing the location of the major components of this experiment. The UCN source is off the picture to the left. The RH dump detector is the primary normalization counter for these results. The dam was used for selected runs and testing.

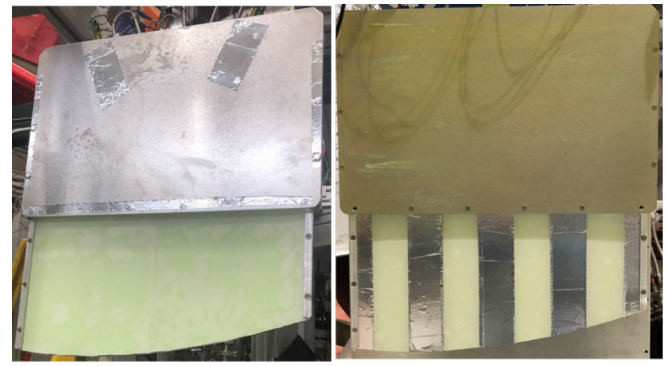

FIG. 3. The photograph on the left shows the dagger called slow and fast (for the slow dagger one side was covered with an aluminum sheet) with wavelength-shifting fibers alternately routed to two PMTs. The dagger on the right is the eight-PMT segmented version.

the trap removes most of the untrappable part of the UCN spectrum, leaving a more relevant range of energies to be counted by the dump detector. Other monitors included one upstream of the RH (gate valve monitor) and one mounted above the trappable UCN height in the RH (active cleaner). We also developed and used several versions of the primary UCN detector (UCN dagger detector) that were lowered into the active volume of the trap to measure surviving neutrons [47].

In the experiment, each run is characterized by a storage time T_{store}. Neutrons are produced by 800 MeV protons delivered to a tungsten spallation target in ~ 0.5 s pulse strings every 5 s during the loading time of 300 s. During this time, a trap door at the bottom of the trap is lowered, and UCN are loaded into the trap. A cleaner to absorb high energy UCN is lowered into the top of the trap to a height of 38 cm from the bottom during the loading time and remains in the trap for an additional cleaning time (typically 50 s) after the trap door is closed. The dagger detector is partially lowered into the top of the trap to help with cleaning; the bottom edge is positioned at the same height as the cleaner at the start of filling and raised above the trap during the storage time, which begins when the cleaner and dagger are raised out of the trap. After the storage time, the dagger detector is typically first lowered to the cleaning position (to search for uncleaned or heated neutrons) and finally lowered to 1cm from the bottom of the trap where it counts stored neutrons for 300 s. These parameters are variable and were changed to perform systematic studies.

We made changes to the dagger throughout the experimental campaigns. These changes were aimed at both increasing the efficiency of the detector and reducing peak count rates. The dagger consists of ^{10}B-coated-ZnS scintillator laminated to an acrylic plate. Wavelength shifting fibers conduct the scintillation light induced by charged particles from the reaction $^{10}\text{B}(\text{n},\alpha)^{7}\text{Li}$ into pairs of photomultiplier tubes (PMTs). Photographs of the daggers used are shown in Figs. 3 and 4.

The small negative Fermi potential of ^{10}B, combined with its high neutron absorption cross section ensures high efficiency for UCN counting. Different thicknesses of ^{10}B, varying from 2 to 120 nm, have been tested and found to give statistically consistent lifetimes but very different counting times. Improved coating techniques produced transparent 120 nm ^{10}B coatings used in the 2020–2022 daggers shown.

In 2020 two detectors were used. The first suffered from a 1.0 Hz background (due to α's from surface contamination of ^{241}Am) that was reduced to 0.2 Hz with new ^{10}B /ZnS sheets on a new dagger. All of the 2020 data and the initial 2021 data were taken with the dagger referred to as Fast,

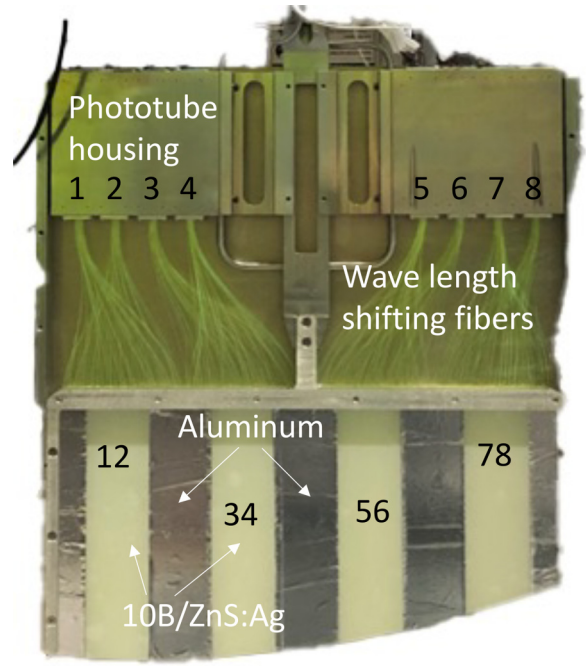

FIG. 4. Photograph of the segmented (high counting rate) dagger described in the text. An aluminum plate that covered the exposed wavelength shifting fibers during data acquisition has been removed for clarity. The eight PMTs are labeled by the top row of black numbers. The strips are labeled by the bottom row of black numbers, each of which corresponds to the PMT pair used for coincidence readout of that strip.

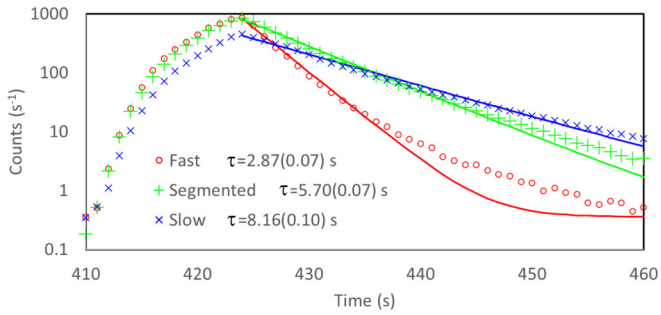

FIG. 5. Unloading curve for each of the daggers described in the text. The data are an average of all the 20 s holding time counting curves for each dagger. The solid curves are single exponential plus constant background fits to the data. A single exponential was used to characterize the main decay component. The unloading times and uncertainties are given in the legend.

denoting the relatively short characteristic time to empty the trap compared to the other daggers. A low-rate ("Slow") version of the new dagger was tested in 2021 by covering half (one complete side) of the detector with UCN-reflective aluminum. In 2020 and 2021 the light was distributed to two PMTs each covering the full dagger. In 2022 the dagger was divided into four vertical sections and utilized eight PMTs, with a pair of PMTs collecting light from each vertical section. This change reduced the maximum count rate in any section of this "Segmented" dagger by about a factor of 4 compared to the Fast dagger. The counting rate was further reduced by replacing part of the active area with aluminum strips (Fig. 4).

Unloading time distributions characterize the detected UCN as a function of time. Histograms depicting the counted UCN as a function of time after dagger motion started for each of these daggers are shown in Fig. 5. For comparison, we include the lifetimes for the daggers used in 2021 and 2022. The resulting lifetimes for fast (2021), segmented (2022), and slow (2021) daggers are, respectively, 879.81 (1.18) s, 876.93 (0.56) s, and 877.94 (0.69) s, where quoted uncertainties are statistical only.

We studied potential systematic effects such as background, UCN loading, uncleaned neutrons, and UCN heating. Monte Carlo-generated pseudo data were used to test different coincidence algorithms and rate-dependent corrections to the UCN counts measured (see analysis section). We also tested inserting variable height barriers (dams) into the Roundhouse (see Fig. 2) for the purpose of increasing the fidelity of the Roundhouse in representing the UCN spectrum ultimately stored in the UCN trap.

III. ANALYSIS

The approach to analyzing these data sets is similar to our previous analysis [6]. Our data are blinded with a blinding factor in the range of 0.99986–1.00171 that hides the actual holding time from analyzers, as described in Ref. [6]. The range of ± 1.5 s was chosen to be several times the uncertainty of our previous measurement. We unblinded our data after achieving agreement between at least three analyzers for each of the three data sets.

Data were taken in octets of runs in a sequence of different holding times chosen to minimize impacts of drifts in normalization (20,1550,1550,50,100,1550,1550,200 s). The number of short and long (1550 s) holding runs was chosen to optimize precision in determining the lifetime. In practice, the number of runs with 1550 s holding time was roughly equal to the total number of the shorter holding time runs.

The elements of the analysis are run selection, event definition, correction for rate dependent effects, calculating a yield normalized to the number of trappable neutrons loaded into the trap, determining a lifetime from the long- and short-hold yields, and finally applying systematic corrections to the lifetime.

IV. EVENT DEFINITION

The data stream consists of ordered lists of time stamps and channel numbers for the monitors and dagger photomultiplier tubes. The monitor detector signals were integrated with timing-filter amplifiers and discriminated, such that a detector hit can be interpreted as a single UCN-absorption event. In the case of the dagger detector, the times of single photoelectrons from each PMT are recorded. The data stream also includes a map of the state of a set of tag bits that mark the state of experimental controls with each time stamp. A UCN event in the dagger detector is defined by time-clustered photon coincidences between pairs of dagger PMTs. We have used different approaches to event definition and tested the impact by analysis of pseudo data to inform our choice.

The search for an event starts with observation of two photons (from different PMTs of a pair) within 100 ns. The photon number is incremented with each additional photon from either PMT of the pair until the time between subsequent photons is greater than 1000 ns. A 20 ns fixed deadtime is built into the event detection to avoid retriggering. The standard for determining a UCN event requires a minimum number of photons during the clustering period. The features above (number of photons, coincidence windows, fixed deadtime) can be varied. The live time during the complete measurement cycle (fill, clean, and unload) is tracked in a time-binned histogram by accumulating the dead time from each UCN event clustering period. We tested various UCN event threshold photon numbers and converged on using ten photons, as it improved signal-to-noise for long holding times with only slight degradation in statistical uncertainty.

Corrections to the UCN histograms are made for the rate-dependent effects of deadtime and photon pileup. At the finish of analyzing a run, the number of coincidence events in each time bin is divided by the livetime for that bin, and the resulting histogram is output as our "unloads" versus time. The data are also corrected for extra photons that are the result of previous events that depend on the UCN rate, the pileup correction. The pileup correction is performed using two methods. The first tracks the instantaneous photon rate, excluding photons within UCN events, and adjusts the photon threshold used to define UCN events to account for the estimated probability of accidental photons within an event. The second uses a model of the photon tail to statistically correct for pileup photons.

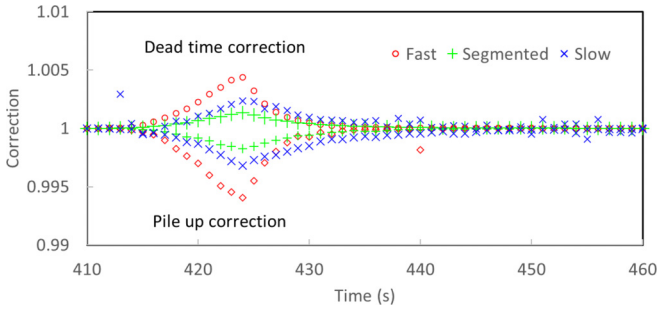

FIG. 6. Example of 20 s holding time deadtime and pileup correction for the average short holding runs as shown in Fig. 5.

A comparison of dead time and pile up corrections for the UCN counting portion of an average of 20 s holding time runs for the different dagger configurations is shown in Fig. 6. These corrections scale with counting rate.

V. RUN SELECTION

"Good" runs were chosen from a large set of production runs. The proton beam used to generate the UCN was occasionally interrupted during trap filling. Runs are eliminated when this led to significant changes in monitor counter ratios or a very small number of loaded UCN. Off-normal conditions in the experiment noted in the logbook also resulted in elimination of runs. Runs that exhibit yields far from others with the same storage time are examined for potential problems and eliminated if warranted. Each analyzer developed and shared their selection criteria. In the end about 90% of the production runs pass the run selection criteria. This number varies for the different analyzers because of different selection criteria. The lifetimes extracted by the different analyzers agreed to within the uncorrelated errors between their data sets.

Runs were divided into major groups for separate lifetime analysis for reasons such as a major change in experimental configuration or a change in blinding factors. Within each of these global lifetime fits the data were divided into smaller groups referred to as epochs. The epochs were used in averaging described later.

VI. CALCULATION OF YIELDS AND LIFETIME FITTING

The analysis uses a histogram of UCN detected (as defined in the Event Definition section) in the dagger detector as a function of time. The sequence of dagger movement before reaching the counting position has been described above in the section on experimental configuration. The histogram has a well-defined peak at the time the dagger is lowered to empty the trap. UCN are integrated over the peak region (usually 60 s) and a background region of the same length starting 50 s after the end of the peak region. For a ten-photon coincidence event, the integrated peak/background ratio is typically greater than 150 for a 1550 s holding time run. Unloading time distributions for different holding times are shown in Fig. 7.

Background is subtracted from the peak, and yields are calculated relative to a monitor (the RH dump detector described earlier) that measures a quantity proportional to the number

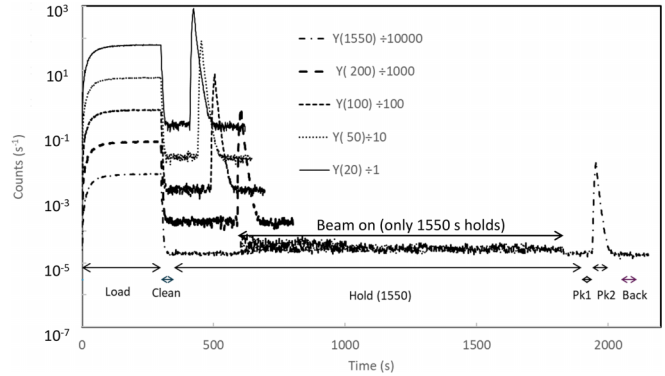

FIG. 7. Average holding time distributions from the 2022 running period. During about half of the long holding time runs, the proton beam was turned on to supply UCN to other experiments. This is reflected in the larger backgrounds labeled in the figure as "Beam on." The counting times (Pk1, Pk2, Back[ground]) are illustrated for the 1550 s sum. In all cases, the holding time starts after cleaning and extends to the beginning of peak 1 (Pk1) counting with the dagger lowered to the cleaning position. The counting times are the same for all holding times.

of UCN loaded into the trap. Yields, $Y_{0,i}$, and uncertainties, $\Delta Y_{0,i}$, for a given run, i, are calculated as follows:

$$Y_{0,i} = \frac{C_{\mathrm{peak},i} - C_{\mathrm{back},i}}{M_i},$$

$$\Delta Y_{0,i} = \frac{1}{M_i}\sqrt{\frac{C_{\mathrm{peak},i} - C_{\mathrm{back},i}}{\mathrm{DQE}^2_{\mathrm{peak}}} + \frac{(C_{\mathrm{peak},i} - C_{\mathrm{back},i})^2}{M_i \times \mathrm{DQE}^2_{\mathrm{Norm}}}}, \quad (2)$$

where $C_{\mathrm{peak},i}$ is the sum of UCN counts in a counting gate beginning at the time the dagger is lowered into its counting position (Pk2), $C_{\mathrm{back},i}$ is the background obtained in the background gate, and M_i is the integrated number of counts measured in the RH Dump Detector at the end of the filling period. The factors $\mathrm{DQE}_{\mathrm{peak}}$ and $\mathrm{DQE}_{\mathrm{norm}}$ are adjusted in the final lifetime fit to give a reduced χ^2 of unity in the lifetime fit (discussed more below). In this work, we have assumed that fluctuations in the loading result in yield fluctuations that are not reflected in the counting uncertainty of M_i, which is small. (For a single run M_i is several times 10^5.) $\mathrm{DQE}_{\mathrm{norm}}$ has been used to account for uncertainty of the initially loaded UCN and has been adjusted using the short holding time runs. The factor $\mathrm{DQE}_{\mathrm{peak}}$ is adjusted in the final lifetime fits to achieve reduced χ^2 of unity. In our previous work, only $\mathrm{DQE}_{\mathrm{norm}}$ was used to scale the yield uncertainty. The differences in the lifetime results with the additional parameter $\mathrm{DQE}_{\mathrm{peak}}$ are small.

The normalization is based on a different UCN velocity spectrum than is stored in the trap after cleaning. We apply a single correction for this effect over sets of runs (epochs) for which the spectrum is nearly constant using a ratio ($R_{\mathrm{mon},i}$) of the RH Dump monitor to a second monitor sensitive to a different UCN energy range than the narrow range stored in the trap. The second monitor used for this correction was the dagger detector during filling (when it was positioned above the trap at the cleaning height). Data with the roundhouse

cleaner removed and with a dam in roundhouse to cut off the low energy part of the spectrum have been used to provide a check of this correction, which has the form:

$$Y_{\mathrm{sc},i} = Y_{0,i}(1 + S_E(R_{\mathrm{mon},i} - \langle R_{\mathrm{mon},i}\rangle))$$
$$\Delta Y_{\mathrm{sc},i} = \Delta Y_{0,i}(1 + S_E(R_{\mathrm{mon},i} - \langle R_{\mathrm{mon},i}\rangle)), \quad (3)$$

where $Y_{0,i}$ is corrected by a small number (S_E) in general different for each epoch E, for each run relative to the average of $R_{\mathrm{mon},i}$ over an epoch. The S_E corrections are chosen to minimize the χ^2 [see Eq. (7)] between $y_{\mathrm{cor},i}$ [Eq. (6)] and the calculated yield $y_{\mathrm{cal},i}$ [Eq. (4)] for the short (< 1550 s) holding time runs in an epoch. The addition of the round house dump detector used to normalize the current data has significantly reduced the sensitivity of the normalization to spectral changes from our previous work. In the 2022 data this correction leads to a reduction in the χ^2 of 158 for 758 short holding time runs and a shift in the lifetime of -31 ms. Although it does not result in a significant lifetime shift it does improve the fit. The yield predicted for a given run, i, for a given storage time, $T_{\mathrm{hold},i}$, and lifetime, τ_{fit} is $y_{\mathrm{cal},i}$:

$$y_{\mathrm{cal},i} = e^{-\left(\frac{T_{\mathrm{hold},i}+\Delta T_{\mathrm{ps},i}}{\tau_{\mathrm{fit}}-\Delta\tau_{\mathrm{pressure},i}-\Delta\tau_{\mathrm{sb},i}}\right)}. \quad (4)$$

We apply correction factors to the lifetime to account for phase space evolution, $\Delta T_{\mathrm{ps},i}$, of the UCN population in the trap, the residual gas pressure in the trap, $\Delta\tau_{\mathrm{pressure},i}$ (which can cause UCN upscattering), and the statistical bias, $\Delta\tau_{\mathrm{sb},i}$, that arises from combining many measurements that follow Poisson statistics. These factors are discussed in the next section.

Degradation of the surface of the solid deuterium (SD_2) of the UCN source results in both reduced output and hardening of the UCN spectrum [49]. We carried out warming and refreezing cycles of the SD_2 multiple times during each running period to keep the source production as high as possible. These time-dependent normalization changes were accounted for with a second averaging using $y_{\mathrm{cal},i}$ to smooth out intermediate, smooth variations (as opposed to step changes) in the monitors. We first select a continuous block (within an epoch) of n runs around run i. Then we take an average of the ratio $(Y_{\mathrm{SC},i}/y_{\mathrm{cal},i})$ for the subset of short holding time (< 1550 s) runs within that block of n runs. Typically, n is 15, and half the runs in that block of 15 will be short holding time runs. This leads to a correction factor, CF_i,

$$\mathrm{CF}_i = \left\langle \frac{Y_{\mathrm{SC},k}}{y_{\mathrm{cal},k}} \right\rangle_n, \quad (5)$$

where k labels the run within the subset, and corrected yields, $y_{\mathrm{cor},i}$,

$$y_{\mathrm{cor},i} = \frac{Y_{\mathrm{sc},i}}{\mathrm{CF}_i}$$
$$\Delta y_{\mathrm{cor},i} = \frac{\Delta Y_{\mathrm{sc},i}}{\mathrm{CF}_i}. \quad (6)$$

This procedure removes any remaining long-term drifts without the need for complete octets. Excluding the long holding time runs from the calculation of CF reduces any possible correlation between the correction factor and the fitted lifetime. This procedure leads to a larger useful data set because accelerator failures in the early filling stage, leading to excluded bad runs, were nonnegligible. The uncertainty, $\Delta y_{\mathrm{cor},i}$, has been propagated from the result of Eq. (2).

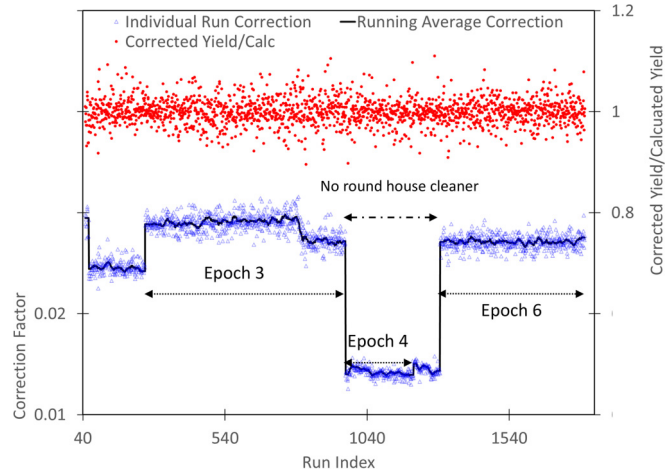

FIG. 8. Normalized and corrected yields from the 2022 data. (Bottom) Blue points: $Y_{\mathrm{SC},i}/y_{\mathrm{cal},i}$, referred to left axis; Black line: correction factor [Eq. (5)]. (Upper) Red points corrected yields [Eq. (6)], referred to right axis. There were six epochs in total; only epochs 3, 4, and 6 are labeled for simplicity.

This procedure is illustrated in Fig. 8 using the data from 2022. The discontinuities between different epochs are visible in the lower plot by vertical changes in the running average. In this plot, based on the work of one analyzer, the large change in epoch 4 is due to removal of the cleaner in the Roundhouse. The other changes between epochs are associated with changes in experimental configuration or electronics. Slow drifts can also be observed. The resulting corrected yields divided by the calculated yields can be seen to be flat across the year's running.

We have characterized the variation within each epoch by calculating the variation in the individual run correction factors. This is shown in Table I for the 2022 dataset, which exhibits variation within an epoch of up to 3%. The standard deviation is larger in Epoch 3 because of the discrete change at the end of the epoch that was due to an adjustment to

TABLE I. The variation in individual correction factors across the various epochs used in data averaging shown in Fig. 8. The statistics shown are the average value over the epoch, the ratio of standard deviation to the average, and the ratio of the difference between the maximum and minimum correction to the average.

Epoch	Average	StDev/Average	(MAX-MIN)/Average
1	0.029	0.000	0.000
2	0.025	0.009	0.040
3	0.029	0.029	0.106
4	0.014	0.018	0.066
5	0.015	0.022	0.075
6	0.027	0.007	0.040

the electronics of the RH dump detector as well as larger run-to-run variations in that region.

The lifetime is fitted to the ensemble $y_{\mathrm{cor},i}$ in the data set. The $y_{\mathrm{cor},i}$ are assumed to be normally distributed, and the value of the lifetime is calculated by minimizing χ^2 [Eq. (7)] of the set. The factor, $\mathrm{DQE}_{\mathrm{peak}}$ [see Eq. (2)], is applied to account for unknown efficiency effects and quality of the fit. The goal is to achieve a reduced χ^2 of 1 and then calculate the statistical uncertainty in τ_{fit} by changing τ to increase the overall χ^2 by 1.

$$\chi^2 = \sum\nolimits_i \left(\frac{y_{\mathrm{corr},i} - y_{\mathrm{cal},i}}{\Delta y_{\mathrm{corr},i}} \right)^2. \tag{7}$$

After unblinding, we discovered an issue that arose from an early fit to a number (about 1%) of runs in the 2020 data set that resulted in a bias that caused the analyzers to exclude runs as statistical outliers because of their large contribution to the χ^2 of the global fit. After unblinding, these runs were found to have a χ^2 contribution below our cutoff threshold of 10. Since there was no reason to exclude these runs, they were added back into the unblinded data set resulting in a 1.0 s shift to the fitted lifetime for a portion the 2020 data set (659 runs), which compares to the 1.0 s statistical uncertainty associated with this subset of data. One analyzer added runs back based on an error in early prescreening based on monitor ratios. The effect on all analyzer's final lifetime for years 2020–2022 was a reduction of approximately 0.14 s.

VII. MEASURED SYSTEMATIC CORRECTIONS TO THE LIFETIME

Systematic corrections are determined from the data for phase space evolution, residual pressure in the trap, and statistical bias introduced when combining runs with different statistical accuracies. These corrections modify the lifetime calculation. The lifetime is fitted with each correction on and off to determine the size of each of these corrections.

The phase space evolution, ΔT_{ps}, is a correction to the storage time of the long holding time runs due to the evolution of the UCN phase space distribution in the trap, which changes the average time it takes a UCN to encounter the lowered dagger. This is determined by calculating the average $\langle X_T \rangle$ of the detection times of the unload counts relative to the time the dagger is lowered over all runs of a given storage time, and correcting the storage time used in the calculation of yield for the long holding time based on the average difference between expected peak position of 1550 s and 20 s runs:

$$\Delta T_{\mathrm{ps},i} = \begin{cases} \langle X_{1550} \rangle - \langle X_{20} \rangle, & i \in \text{Long Holds}, \\ 0, \ \text{otherwise}. \end{cases} \tag{8}$$

This shift is applied to each of the 1550 s holding time runs as shown in Eq. (4) and is less than 0.01 s with a negligible uncertainty.

The pressure correction, $\Delta\tau_{\mathrm{pressure},i}$ is based on published cross section measurements [50,51]. The correction uses the measured pressure (P) in the trap for each run:

$$\Delta\tau_{\mathrm{pressure}} = 3.38 \times 10^5 \frac{s}{\mathrm{torr}} P(\mathrm{torr}). \tag{9}$$

A residual gas analyzer (RGA) was used to monitor the residual gas makeup periodically through the run. The RGA was not run continuously because of the possibility that light from the RGA could be detected in the dagger. After the initial pump down, the residual gas makeup was dominated by water. As the pressure dropped, this gradually shifted to air being the major contaminant. The correction was applied to each run based on the trap pressure for that run and assuming it to be water. An uncertainty of 50% was applied for this correction to cover uncertainties in the contaminant species and the pressure measurement.

The final correction is based on the well-known effect in averages resulting from many data sets that are Poisson distributed. Smaller numbers have smaller absolute errors and are weighted more heavily in a weighted average. This lowers the long holding time yield relative to the short holding time yield which results in a systematically shorter extracted lifetime. This is the statistical bias correction, $\Delta\tau_{\mathrm{SB}}$. The correction is applied in the calculated lifetime as shown in Eq. (4) above. The value of $\Delta\tau_{\mathrm{SB}}$ is determined by a model data set consisting of 1536 runs comprising 192 octets (described above). For each octet, a Poisson-distributed random number of counts was chosen from a distribution with mean given by

$$N = N_0 e^{-\frac{t_{\mathrm{hold}}}{\tau_{\mathrm{mc}}}}. \tag{10}$$

The octets were analyzed using the same procedure as with the production runs to obtain a fitted lifetime. This includes renormalizing each octet using ratios to the predicted lifetime. The entire simulated data set is then fitted to obtain a biased lifetime, τ_{biased}. This procedure is repeated 10 000 times and the fitted average lifetime is subtracted from the lifetime assumed in the Monte Carlo, $\tau_{\mathrm{mc}} = 877.75$ s, to obtain the statistical bias. The uncertainty in τ_{fit} was calculated using the standard deviation of the result over the 10 000 trials.

This procedure is repeated to generate results for a range of N_0. The difference between the Monte Carlo lifetime and the fitted biased lifetime is fitted as a function of N_0 using a power law:

$$\Delta\tau_{\mathrm{sb}} = a N_0^{\left(b + \frac{c}{N_0}\right)}. \tag{11}$$

The parameters used for a, b, and c are (2985.3 s, −1.00102, and 0.855). When the performance of the UCN source improved, N_0 increased, decreasing the correction. In practice, different functional fits to the statistical bias Monte Carlo result in equivalent statistical bias corrections. The c term in the power law is needed to produce good agreement for the smallest values of N_0 (< 1000), which are only seen when vertical sections in the 2022 dagger are analyzed separately. For the data presented in this paper, the statistical bias correction was between 0.4 and 0.5 s.

VIII. UCN HEATING AND COOLING

The depth of the trap is 45 cm, and UCN are cleaned to the height of 38 cm. Neutrons with energies above 45 neV, which corresponds to neutrons that can reach a vertical height of 45 cm, can eventually escape the trap if the cleaning is insufficient. If these neutrons escape the trap during the long holding period, then the lifetime of neutrons in the

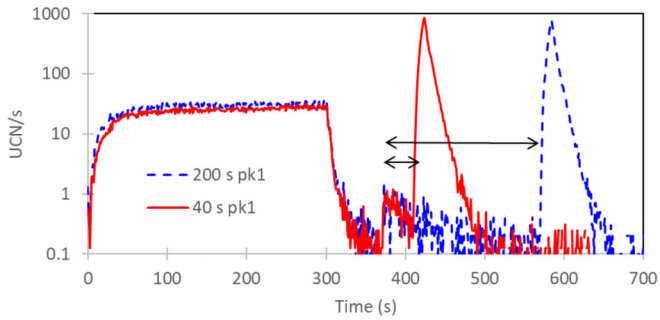

FIG. 9. Average counting time distribution for 2022 short holding time runs with no cleaning with a 40 s long Pk1 counting time (red solid line) and with 200 s long Pk1 counting time (blue dashed line). The arrows show the Pk1 integration gates used for this analysis.

trap will be shorter than the neutron lifetime. UCN that are vibrationally heated can also escape the trap at later times. Both of these processes, which are estimated to be small in Ref. [52], can lead to trap lifetimes that differ from the free neutron lifetime. Our analysis assumes that the population of quasibound neutrons that leave the trap scales linearly with the Pk1 signal. Under normal loading and cleaning conditions, neutrons that are in the Pk1 region are still trapped, and losses from these neutrons are negligible [52]. We therefore take our linear scaling as an upper limit for potential losses tied to detected neutrons in the Pk1 region. These effects can both be experimentally limited using the first counting period (Pk1) when the dagger is moved to the cleaning position before being lowered to the bottom of the trap.

We have taken data without lowering the cleaner ("uncleaned") to determine the losses experienced when UCN are not properly cleaned, as in Ref. [6]. The measured lifetime for uncleaned runs is significantly shorter due to UCN above the cleaning height. The observed losses are scaled for the relative magnitude of the Pk1 signal to account for the significant difference in populations above the cleaning height determining the systematic uncertainty for uncleaned UCN.

Unloading time distributions for 20 s holding time runs without cleaning (i.e., in which the cleaner was never lowered into the trap prior to the holding period) are shown in Fig. 9. The peak of high energy UCN remaining in the uncleaned distributions (Pk1, dagger lowered to the cleaning position) show a tail that extends under the normal second counting period (Pk2 with the dagger 1 cm above the bottom of the trap). The fraction of counted neutrons has been estimated by taking data with a longer Pk1 counting time of 200 s. The ratio of background subtracted counts in first 200 s of Pk1 to those in the first 40 s (the duration the dagger is held in this position in production runs) is 1.76(0.15) and has been used to correct the net counts in Pk1 in the production data to arrive at the uncertainties for inefficient cleaning and heating given in Table II. The gap between the cleaning height and the full trap height leads to a short counting time for unbound UCN in this region.

IX. IMPACTS OF PHASE SPACE EVOLUTION AND DAGGER NONUNIFORMITY

The UCNτ trap is designed with a built-in asymmetry to mix the neutron orbits to rapidly populate all the available phase space in the trap [53]. However, detailed Monte Carlo studies [52] have shown that the process of filling the phase space is somewhat slower than originally expected. For example, neutrons loaded into the trap must have vertical momentum to move into the trap, clearly leaving some parts of phase space initially unoccupied. Over time, neutrons evolve into the unoccupied phase space.

In our previous work, we accounted for phase space evolution by using the measured mean UCN unload time for long holding time runs [see Eq. (8)] rather than the programmed unload time in the lifetime fitting. Although this requires a small correction to the lifetime, it introduces a negligible systematic uncertainty. In the 2022 data from this work, the segmented dagger (Fig. 4) provided additional information about phase space evolution. We measured independent lifetimes for each of the dagger segments and found that the fitted lifetime across the dagger segments varies by about 10 s (Fig. 10). The lifetime found from the shortest strip (78), which does not reach as far into the trap as the longer strips, is the shortest. We interpret this as due to phase space mixing, which causes the distribution of the neutrons in the trap to move over time. This phase space evolution, coupled with

TABLE II. Systematics corrections and uncertainties calculated for each year's data set. Numbers shown are an averages of the different analyzers' individual corrections and uncertainties. The "heating" and "uncleaned" corrections are a weighted average of those in this work and Ref. [6]. All numbers are given in seconds.

	2020		2021 Fast		2021 Slow		2022		Average	
Effect	Corr.	Unc.	Corr.	Unc.	Corr.	Unc.	Corr.	Unc.	Corr.	Unc.
Event definition	0.00	0.20	0.00	0.16	0.00	0.17	0.00	0.14	0.00	±0.16
Dagger uniformity	0.00	0.02	0.00	0.02	0.00	0.02	−0.22	0.02	0.06	±0.02
Residual gas	0.06	0.03	0.07	0.04	0.04	0.02	0.05	0.03	0.05	±0.03
Statistical bias	0.51	0.01	0.50	0.01	0.55	0.01	0.31	0.01	0.47	±0.01
Depolarization	0.00	0.07	0.00	0.07	0.00	0.07	0.00	0.07	0.00	+0.07
Uncleaned	0.00	0.01	0.00	0.01	0.00	0.01	0.00	0.01	0.00	+0.01
Heating	0.00	0.07	0.00	0.07	0.00	0.07	0.00	0.07	0.00	+0.07
Δt_{ph}	−0.02	0.02	−0.01	0.01	−0.02	0.01	−0.04	0.01	−0.02	±0.01
Uncorrelated sum									0.58	+0.20−0.17

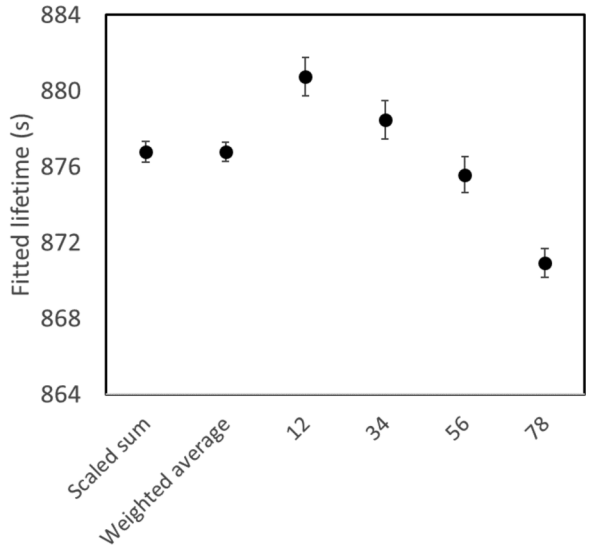

FIG. 10. 2022 lifetime fits comparing the results from the four different strips with the analysis of the scaled sum and weighted average. The four strips (12, 34, 56, 78) are shown from left to right in Fig. 3.

variation in the efficiency of the dagger sections, could cause a systematic error in the lifetime determined by summing over the entire dagger. The gains of the sections of the segmented dagger, when measured using the distribution of the number of photoelectrons from each section, varied by 20%. Effectively balancing the gains by scaling the photon thresholds for each segment reduced the fitted lifetime by 0.22 s (Scaled sum in Fig. 10). The lifetime reported here uses balanced gains for the 2022 data set. This interpretation is supported by ongoing Monte Carlo modelling [52].

There is only a small shift in the ratio of the long to short holding time unloaded counts as a function of time as the dagger is moved into the trap, Fig. 11. Similar plots for the individual dagger strips show similar ratios vs. time. This indicates that there is very little vertical phase space evolution. A change in the vertical distribution between long and short

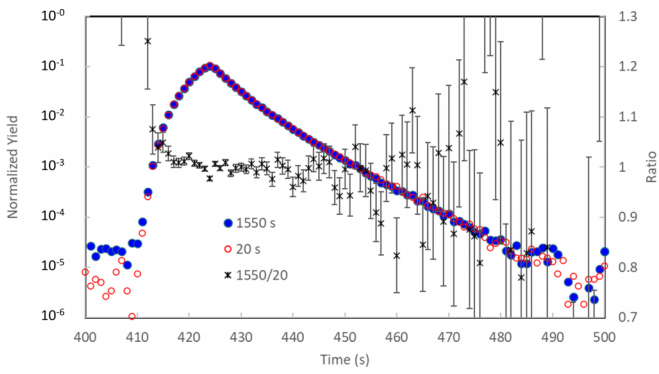

FIG. 11. Normalized short (red open) and long (blue closed) unloading curves plotted on the left axis and the ratio, plotted on the right axis. The elapsed time of the long-hold points have been shifted by the difference in long and short holding times (1550–20 s) to overlap with the short-hold points.

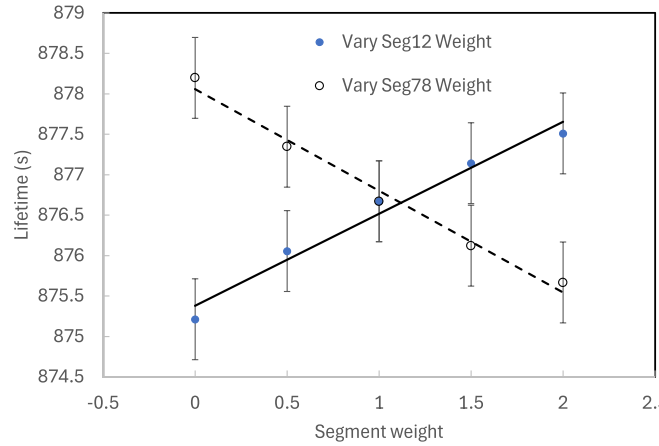

FIG. 12. A plot of the lifetime as a function of changes in the weighting of the effective gains of the two outer segments. The lines show the slopes of the two curves used to estimate the horizontal phase space evolution uncertainty.

holding time would be reflected in a shift in the centroid of the time distributions, which is measured to be less than 0.04 s. These shifts have been included in the lifetime fits as a shift in the holding time.

If all the neutrons are counted, then phase space evolution would not affect the measured lifetime. However, if different parts of the dagger have different efficiencies that bias the counting as a function of position, then they will bias the lifetime determination. To estimate the size of this systematic uncertainty, the light output from the daggers was mapped using a laser to excite the wavelength shifting fibers. The maps show that the relative dagger efficiency has top to bottom efficiency changes of less than 3%. We changed the weighting of the different dagger segments (Fig. 12) and refitted the lifetime to estimate the uncertainty introduced by nonuniformities in the horizontal dagger efficiency.

We find that these gain variations introduce a systematic uncertainty of 0.02 s (listed in Table II).

X. RESULTS AND CONCLUSION

Four different analysis teams prepared results for this publication. Each team worked on data from various years, and we ensured there would be at least three independent analyses that agree within the uncorrelated error for each year. The lifetime results for each year are the average of all the independent results (τ_A, τ_B, τ_C, and τ_D) for that year, with a statistical uncertainty chosen as the average of the uncertainties estimated by individual analyzers ($d\tau_A$, $d\tau_B$, $d\tau_C$, and $d\tau_D$). The combined lifetime in Table III is the error-weighted average of each year's results with uncertainty given by weighted standard mean.

Each team studied various systematic corrections mentioned in the Analysis section earlier, and the size of each correction is reported in Table II along with the average of the systematic uncertainties estimated by each team for each year. The statistical-bias correction (~ 0.5 s) is the largest systematic correction. Table II also reports the average of

TABLE III. Unblinded neutron lifetime results by different analysis teams (A, B, C, and D) for each year and the combined result. The previous published results from Ref. [6] are included in the global average.

Analysis	A	B	C	D	Average
2017 Ref. [6]	877.68 ± 0.30	877.78 ± 0.34	877.74 ± 0.33		877.73 ± 0.32
2018 Ref. [6]	878.06 ± 0.49	877.80 ± 0.46	877.55 ± 0.55		877.80 ± 0.50
2020	879.47 ± 0.86	879.38 ± 0.92	879.32 ± 0.90		879.39 ± 0.89
2021	878.41 ± 0.60	878.40 ± 0.59	878.41 ± 0.55		878.41 ± 0.58
2022	876.81 ± 0.56	876.78 ± 0.58	877.06 ± 0.53	877.08 ± 0.63	876.93 ± 0.57
Current					877.96 ± 0.37
Global					877.83 ± 0.22

systematic uncertainties stemming from each team's event definition parameters, and it is the largest contributor to the systemic uncertainty in the reported lifetime, followed by the systematic uncertainty from the residual uncleaned or heated UCNs in the trap. Varying the event definition parameters (event length, counting length, and threshold) yields a distribution of lifetimes; the uncertainty reported is 1σ of that distribution.

XI. DISCUSSION

The results of this analysis have been included in a global analysis that includes data from the previous two UCNτ measurements [6]. The result, plotted in Fig. 13, shows good agreement with each year's analysis. The p value comparing the combined result with the individual year results is 14%. Our combined result for the free neutron lifetime measured with UCNτ trapdoor loading is 877.83 ± 0.22 (statistical)+0.20–0.17 (systematic) s. The systematic uncertainty is taken from the quadratic sum of the average values reported in Table II. We have taken the systematic uncertainties from the current analysis to apply to the previous data.

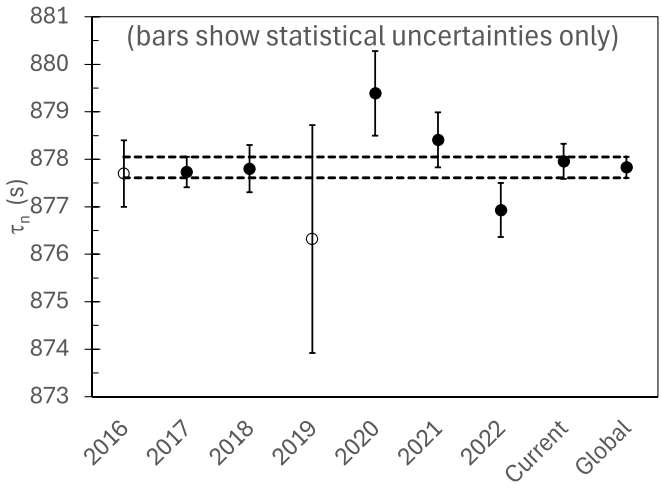

FIG. 13. The global analysis (horizontal lines) compared to the individual year's results for all the included data. The point labeled "Current" is the weighted average of the 2020–2022 datasets discussed in the present paper. The "Global" result additionally includes the previously published [6] 2017–2018 datasets. The open symbols for the 2016 and 2019 datasets are from Refs. [45,54], respectively, and are not included in the global result.

The plot in Fig. 13 includes a result from a measurement in which the neutrons were counted by emptying them by opening the trap door and counting them in a detector under the trap, the so called fill and dump method [54]. The two methods of counting the neutrons give consistent results. The earlier result in Ref. [45] is also plotted though not included in the global analysis, as the identified leading systematic uncertainties are different between that and the present result.

XII. PLANNED UPGRADES TO THE UCNτ APPARATUS: UCNτ+

This paper presents the final neutron lifetime from the Los Alamos UCN facility magneto-gravitational trap using loading through the trap door, UCNτ. With the current counting techniques and given the number of UCN loaded into the experiment through the trap door, it is difficult to obtain better statistical or lower systematic uncertainties. Work is underway to replace the trapdoor-based loading with an elevator loading method that is expected to improve the loaded number of UCN by a factor of 5–10. The largest systematic uncertainty in present measurements arises from the event definition. We are currently developing a new screen scintillator based on cerium doped yttrium aluminum perovskite (YAP:Ce) that, with a suitable wavelength shifter, provides similar light output to ZnS:Ag but without the long fluorescence tail. Events will be defined from coincidence of light produced within the 40 ns decay time of the YAP:Ce. This compares to the average event width of about 4 μs with the ZnS:Ag detector and should provide at least a factor of 10 reduction in the driving systematic uncertainty in this work. With these improvements it should be possible to approach a total uncertainty of 0.10 s.

ACKNOWLEDGMENTS

The authors thank the staff and management of the Los Alamos Neutron Science Center for providing the UCN used for these experiments and the Los Alamos LDRD program, the U.S. Department of Energy, Office of Science, Office of Nuclear Physics under Awards No. DE-FG02-ER41042, No. DE-AC52-06NA25396, No. DE-AC05-00OR2272, and No. 89233218CNA000001 under proposal LANLEEDM; NSF Grants No. 1614545, No. 1914133, No. 1553861, No. 2310015, No. 1812340, No. 1714461, No. 2110898, No. 1913789, No. 2209521, No. 2209481 and No. 2210341.

[1] G. J. Mathews, T. Kajino, and T. Shima, Phys. Rev. D **71**, 021302(R) (2005).
[2] D. Dubbers and M. G. Schmidt, Rev. Mod. Phys. **83**, 1111 (2011).
[3] M. Gonzalez-Alonso, O. Naviliat-Cuncic, and N. Severijns, Prog. Part. Nucl. Phys. **104**, 165 (2019).
[4] A. N. Ivanov, M. Pitschmann, and N. I. Troitskaya, Phys. Rev. D **88**, 073002 (2013).
[5] S. Navas, C. Amsler, T. Gutsche, C. Hanhart *et al.*, Phys. Rev. D **110**, 030001 (2024).
[6] F. M. Gonzalez, E. M. Fries, C. Cude-Woods, T. Bailey *et al.*, Phys. Rev. Lett. **127**, 162501 (2021).
[7] A. Saunders, M. Makela, Y. Bagdasarova, and H. Back *et al.*, Rev. Sci. Instrum. **84**, 013304 (2013).
[8] T. M. Ito, E. R. Adamek, N. B. Callahan, J. H. Choi *et al.*, Phys. Rev. C **97**, 012501 (2018).
[9] F. E. Wietfeldt and G. L. Greene, Rev. Mod. Phys. **83**, 1173 (2011).
[10] A. T. Yue, M. S. Dewey, D. M. Gilliam, G. L. Greene, A. B. Laptev, J. S. Nico, W. M. Snow, F. E. Wietfeldt *et al.*, Phys. Rev. Lett. **111**, 222501 (2013).
[11] K. Hirota, G. Ichikawa, S. Ieki, and T. Ino *et al.*, Progr. Theor. Exper. Phys. **2020**, 123C102 (2020).
[12] J. T. Wilson, D. J. Lawrence, P. N. Peplowski, V. R. Eke, J. A. Kegerreis *et al.*, Phys. Rev. C **104**, 045501 (2021).
[13] A. Czarnecki, W. J. Marciano, and A. Sirlin, Phys. Rev. Lett. **120**, 202002 (2018).
[14] C.-Y. Seng, M. Gorchtein, H. H. Patel, and M. J. Ramsey-Musolf, Phys. Rev. Lett. **121**, 241804 (2018).
[15] Y. Aoki, T. Blum, G. Colangelo, and S. Collins *et al.*, Eur. Phys. J. C **82**, 869 (2022).
[16] A. Czarnecki, W. J. Marciano, and A. Sirlin, Phys. Rev. D **100**, 073008 (2019).
[17] L. Hayen, Phys. Rev. D **103**, 113001 (2021).
[18] C.-Y. Seng, M. Gorchtein, and M. J. Ramsey-Musolf, Phys. Rev. D **100**, 013001 (2019).
[19] M. Gorchtein and C.-Y. Seng, Universe **9**, 422 (2023).
[20] V. Cirigliano, W. Dekens, E. Mereghetti, and O. Tomalak, Phys. Rev. D **108**, 053003 (2023).
[21] V. Cirigliano, D. Díaz-Calderón, A. Falkowski, and M. González-Alonso *et al.*, J. High Energy Phys. 04 (2022) 152.
[22] V. Cirigliano, A. Crivellin, M. Hoferichter, and M. Moulson, Phys. Lett. B **838**, 137748 (2023).
[23] V. Cirigliano, W. Dekens, J. de Vries, and E. Mereghetti *et al.*, J. High Energy Phys. 03 (2024) 033.
[24] T. Aaltonen, S. Amerio, D. Amidei, and A. Anastassov *et al.*, Science **376**, 170 (2022).
[25] B. Belfatto and S. Trifinopoulos, Phys. Rev. D **108**, 035022 (2023).
[26] O. Fischer, B. Mellado, S. Antusch, and E. Bagnaschi *et al.*, Eur. Phys. J. C **82**, 665 (2022).
[27] D. Marzocca and S. Trifinopoulos, Phys. Rev. Lett. **127**, 061803 (2021).
[28] A. Falkowski, M. González-Alonso, and O. Naviliat-Cuncic, J. High Energy Phys. 04 (2021) 126.
[29] J. C. Hardy and I. S. Towner, Phys. Rev. C **102**, 045501 (2020).
[30] J. S. Nico, M. S. Dewey, D. M. Gilliam, and F. E. Wietfeldt *et al.*, Phys. Rev. C **71**, 055502 (2005).
[31] A. Serebrov, V. Varlamov, A. Kharitonov, and A. Fomin *et al.*, Phys. Lett. B **605**, 72 (2005).
[32] A. Pichlmaier, V. Varlamov, K. Schreckenbach, and P. Geltenbort, Phys. Lett. B **693**, 221 (2010).
[33] A. Steyerl, J. M. Pendlebury, C. Kaufman, S. S. Malik, A. M. Desai *et al.*, Phys. Rev. C **85**, 065503 (2012).
[34] S. Arzumanov, L. Bondarenko, S. Chernyavsky, and P. Geltenbort *et al.*, Phys. Lett. B **745**, 79 (2015).
[35] A. P. Serebrov, E. A. Kolomensky, A. K. Fomin, I. A. Krasnoshchekova *et al.*, Phys. Rev. C **97**, 055503 (2018).
[36] V. Ezhov, A. Andreev, G. Ban, and B. Bazarov *et al.*, JETP Lett. **107**, 671 (2018).
[37] G. L. Greene and P. Geltenbort, Sci. Am. **314**, 36 (2016).
[38] B. Fornal and B. Grinstein, Phys. Rev. Lett. **120**, 191801 (2018).
[39] G. Baym, D. H. Beck, P. Geltenbort, and J. Shelton, Phys. Rev. Lett. **121**, 061801 (2018).
[40] D. McKeen, A. E. Nelson, S. Reddy, and D. Zhou, Phys. Rev. Lett. **121**, 061802 (2018).
[41] J. Ellis, G. Hütsi, K. Kannike, L. Marzola, M. Raidal, V. Vaskonen *et al.*, Phys. Rev. D **97**, 123007 (2018).
[42] X. Sun, E. Adamek, B. Allgeier, and M. Blatnik *et al.*, Phys. Rev. C **97**, 052501 (2018).
[43] Z. Tang, M. Blatnik, L. J. Broussard, J. H. Choi *et al.*, Phys. Rev. Lett. **121**, 022505 (2018).
[44] M. Le Joubioux, H. Savajols, W. Mittig, and X. Fléchard *et al.*, Phys. Rev. Lett. **132**, 132501 (2024).
[45] R. Pattie, Jr., N. Callahan, C. Cude-Woods, and E. Adamek *et al.*, Science **360**, 627 (2018).
[46] D. J. Salvat, E. R. Adamek, D. Barlow, J. D. Bowman *et al.*, Phys. Rev. C **89**, 052501(R) (2014).
[47] C. Morris, E. Adamek, L. Broussard, and N. Callahan *et al.*, Rev. Sci. Instrum. **88**, 053508 (2017).
[48] Z. Wang, M. Hoffbauer, C. Morris, and N. Callahan *et al.*, Nucl. Instrum. Methods. Phys. Res. A **798**, 30 (2015).
[49] A. Anghel, T. Bailey, G. Bison, and B. Blau *et al.*, Eur. Phys. J. A **54**, 148 (2018).
[50] S. J. Seestrom, E. R. Adamek, D. Barlow, L. J. Broussard *et al.*, Phys. Rev. C **92**, 065501 (2015).
[51] S. J. Seestrom, E. R. Adamek, D. Barlow, and M. Blatnik *et al.*, Phys. Rev. C **95**, 015501 (2017).
[52] N. Callahan, C.-Y. Liu, F. Gonzalez, and E. Adamek *et al.*, Phys. Rev. C **100**, 015501 (2019).
[53] P. Walstrom, J. Bowman, S. Penttila, and C. Morris *et al.*, Nucl. Instrum. Methods. Phys. Res. A **599**, 82 (2009).
[54] C. Cude-Woods, F. M. Gonzalez, E. M. Fries, T. Bailey *et al.*, Phys. Rev. C **106**, 065506 (2022).